



A Possible X-ray Quasi-periodic Oscillation in the Narrow-line Seyfert 1 Galaxy Mrk 142

Xiao-Gu Zhong¹, Jian-Cheng Wang², Yong-Yun Chen¹, and Xiao-Ling Yu¹

¹ College of Physics and Electronic Engineering, Qujing Normal University, Qujing 655011, China; guqian29@yeah.net

² Yunnan Observatories, Chinese Academy of Sciences, Kunming 650216, China

Received 2023 November 28; revised 2024 March 23; accepted 2024 April 16; published 2024 May 29

Abstract

A possible quasi-periodic oscillation (QPO) at frequency 7.045×10^{-5} Hz is found in the narrow-line Seyfert 1 galaxy Mrk 142 in the data of XMM-Newton collected on 2020 April 11. We find that the QPO signal is statistically significantly larger than the 5σ level and highly coherent with quality factor $Q > 5$ at the 0.3–10 keV band by using the method of the Lomb–Scargle Periodogram, the Weighted Wavelet Z-transform and the REDFIT. We analyze the data in 0.3–0.6 keV, 0.6–1 keV, 1–3 keV and 3–10 keV energy bands, and find obvious QPO signals at 0.3–0.6 keV and 1–3 keV bands. We then analyze the time-average spectra and time variability at the QPO frequency of 7.045×10^{-5} Hz, and use a model to fit them. We find that the QPO signal mainly comes from the X-ray hot corona.

Key words: X-rays: galaxies – galaxies: Seyfert – accretion – accretion disks – radiation mechanisms: general

1. Introduction

The nuclei of some galaxies could release enormous energy larger than the sum of their host galaxies. It is so called as Active Galactic Nuclei (AGNs). The most efficient energy production mechanism is commonly believed to be from the matter accreting into supermassive black holes at the center of active galaxies, which could emit the electromagnetic radiation covering the broad band spectrum from radio to gamma-ray bands. Particularly, X-rays could help us to explore the inner construction of AGNs. The X-ray continuum is generally considered to be from the inverse Compton scattering of the soft photons emitted from accretion disk in the hot corona. In the soft X-ray band, the soft excess is a common component in most type 1 AGNs which have low inclinations toward us (Porquet et al. 2004). However, the origin of the soft excess is not well understood so far. Therefore, the time series analysis could probe the inner construction of AGNs in detail. One of the most interesting research questions is the quasi-periodic oscillation (QPO), which could appear in the optical, X-ray and γ ray bands of various classes of AGNs (Espaillat et al. 2008; Gierliński et al. 2008; Gupta et al. 2009; Lachowicz et al. 2009; King et al. 2013; Lin et al. 2013; Fan et al. 2014; Sandrinelli et al. 2014; Ackermann et al. 2015; Graham et al. 2015; Bhatta et al. 2016; Pan et al. 2016; Sandrinelli et al. 2016; Bhatta 2017; Li et al. 2017; Xiong et al. 2017; Zhang et al. 2017; Hong et al. 2018; Zhang et al. 2018; Mancuso et al. 2019; Kushwaha et al. 2020; Li et al. 2021; Yang et al. 2021; Zhang & Wang 2021; Zhang et al. 2021). However, the X-ray QPOs are rare in AGNs, and the unambiguous QPO signal was detected in the NLS1 galaxy RE J1034+396 with $f_{\text{QPO}} = 2.7 \times 10^{-4}$ Hz

(Gierliński et al. 2008; Alston et al. 2014; Hu et al. 2014; Jin et al. 2020). Generally, the QPOs have been detected in the black hole X-ray binaries (BHXBs) because their QPO frequencies determined by the scales of BHXBs are higher than that of AGNs and are suitable for many observation devices. Fortunately, the NLS1 galaxies with lower mass black holes and higher accretion rates give us the opportunity to detect the QPOs by some observation devices, such as XMM-Newton (Jansen et al. 2001) which is the high earth orbit satellite and could provide sufficient exposure time to probe the QPOs in AGNs. Except RE J1034+396, several NLS1 galaxies were also detected QPOs but with lower significance level, such as 1H 0707-495 (Pan et al. 2016; Zhang et al. 2018), Mrk 766 (Zhang et al. 2017), MCG-06-30-15 (Gupta et al. 2018), and MS 2254.9-3712 (Alston et al. 2015) where the QPO was detected in the 1.2–5.0 keV band with the confidence level 3.3σ . Some type 2 Seyfert galaxies were also reported to have the QPOs, such as 2XMMJ12303+110648 (Lin et al. 2013) and XMMUJ134736+173403 (Carpano & Jin 2018). It is interesting to search the QPOs in AGNs because the common nature of the accretion process could exit from BHXBs with a few solar masses to AGNs with larger masses. It's believed for the QPOs to be related with the properties about black holes, such as mass and spin. However, the origin of the QPO is debated so far.

In this work, we report a possible QPO signal in NLS1 Mrk 142 at $\sim 7.045 \times 10^{-5}$ Hz with a confidence level of $\sim 5\sigma$ in the 0.3–10 keV energy band only using XMM-Newton observation on 2020 April 11 with an exposure time of 60ks.

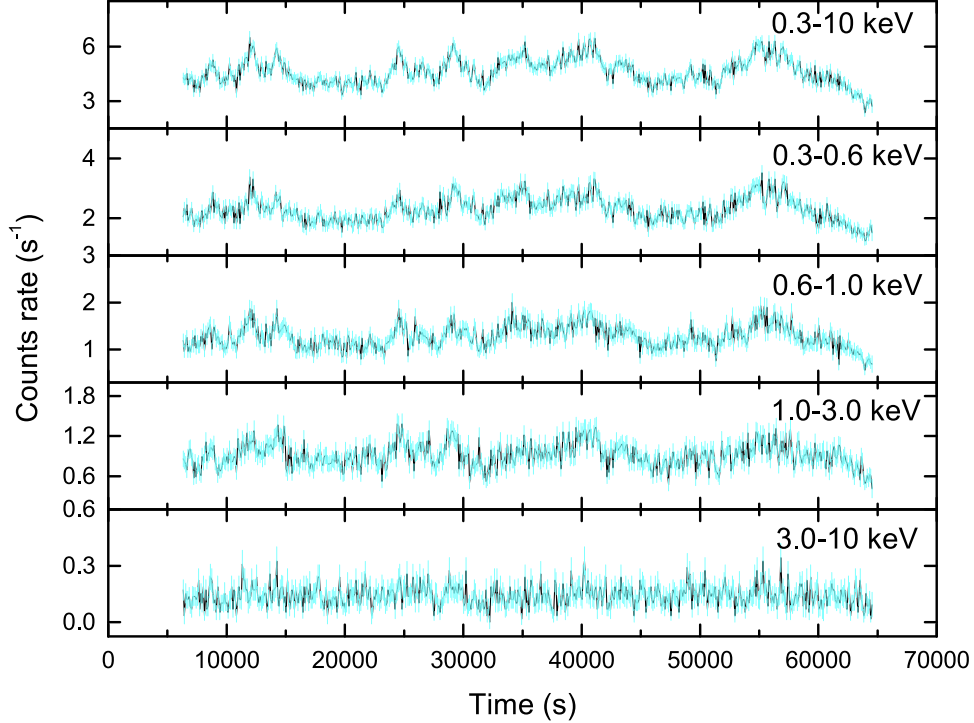


Figure 1. The light curves of 0.3–10 keV, 0.3–0.6 keV, 0.6–1 keV, 1–3 keV and 3–10 keV from top to bottom panels.

The paper is organized as follows. In Section 2, we present the observational data. In Section 3, we analyze the light curve data and show the main results. In Section 4, we analyze the time-averaged spectra and explore the variability properties of the QPO. Finally, we discuss our results and conclusions in Section 5.

2. XMM-Newton Data Reduction

Mrk 142 (a.k.a. PG 1022+519) is a super-Eddington NLS1 galaxy with a low redshift $z = 0.045$, which has a black hole mass of $\log(M/M_{\odot}) = 6.23_{-0.45}^{+0.26}$, and a dimensionless accretion rate of $\dot{M} = \dot{m}c^2/L_{\text{edd}} = 250$ (Li et al. 2018). We choose X-ray data observed by XMM-Newton for Mrk 142 (The observation ID: 0 852 060 301), and only use the EPIC-pn data in 0.3–10 keV to do spectral and time analysis because the MOS1 and MOS2 light curve data have many zero-points which will distort the power spectral density (PSD). The raw data are processed from Observation Data Files following standard procedures based on the Science Analysis System (SAS v21.0.0) and the latest calibration files. The spectra and light curves are extracted using tool *evselect* with default pattern selected. We extract the source spectra and light curves from a circular region with a radius of $30''$ centered on the source. The background spectra are taken from a circular region of the same size near the source. *rmfgen* and *arfgen* are used to produce response matrices. Source spectra are rebinned by

grppha with a minimum of 30 counts per bin. *epiclccorr* is used to correct the light curve. We choose a bin time of 100 s and discard the first 6.25ks of the light curve because there are some flares in the background. The light curves are shown in Figure 1 for 0.3–10 keV, 0.3–0.6 keV, 0.6–1 keV, 1–3 keV and 3–10 keV bands from top to bottom panels, respectively. We test the pile-up for these data by using *epatplot* and find that the pile-up is not important to Mrk142.

3. The X-ray QPO

We first study the power spectra of the total energy band of 0.3–10 keV obtained by the Lomb–Scargle Periodogram (LSP) (Lomb 1976; Scargle 1982). we use the method of Emmanoulopoulos et al. (2013) to evaluate the significance of the QPO signal. The power spectral function $P(f) = Af^{-1}[1 + (f/f_{\text{bend}})^{\alpha-1}]^{-1} + C$ is used (González-Martín & Vaughan 2012), where A , α , f_{bend} and C represent the normalization, spectral index above the band, bending frequency and Poisson noise level respectively. We calculate the 4σ and 5σ significance curves by simulating 10^5 artificial light curves shown in Figure 2. It shows a significant peak at the frequency $\sim 7.045 \times 10^{-5}$ Hz than the 5σ significance level. Then, we use the Weighted Wavelet Z-transform (WWZ) method (Foster 1996) to test the QPO signal. The left panel of Figure 3 shows the 2D plane contour plotting for the WWZ power spectrum. The right panel of Figure 3 shows the

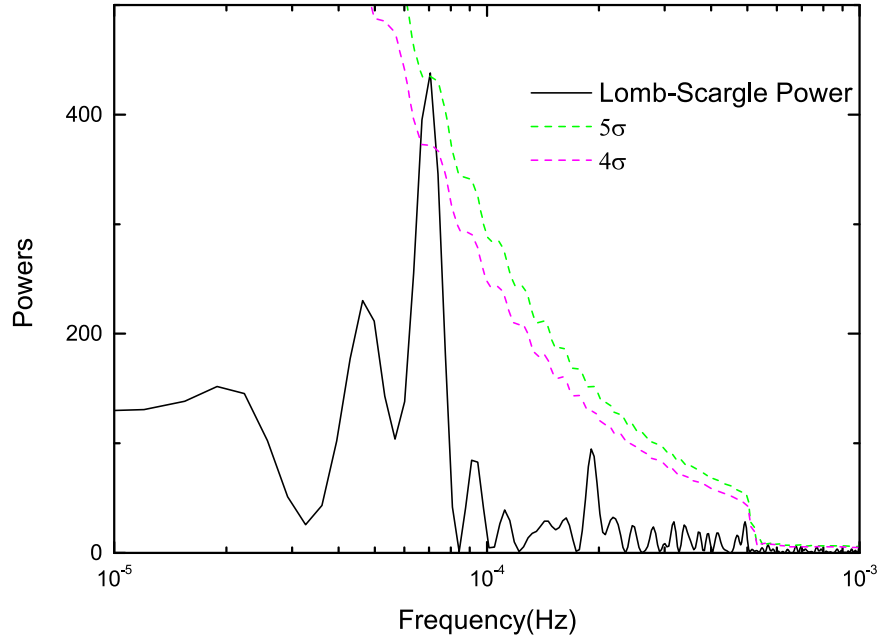


Figure 2. LSP power spectra of the total energy band of 0.3–10 keV are shown in the black solid line. The 4σ (pink dashed line) and 5σ (green dashed line) significance level curves are calculated based on the simulation of 10^3 light curves with the method of Emmanoulopoulos et al. (2013).

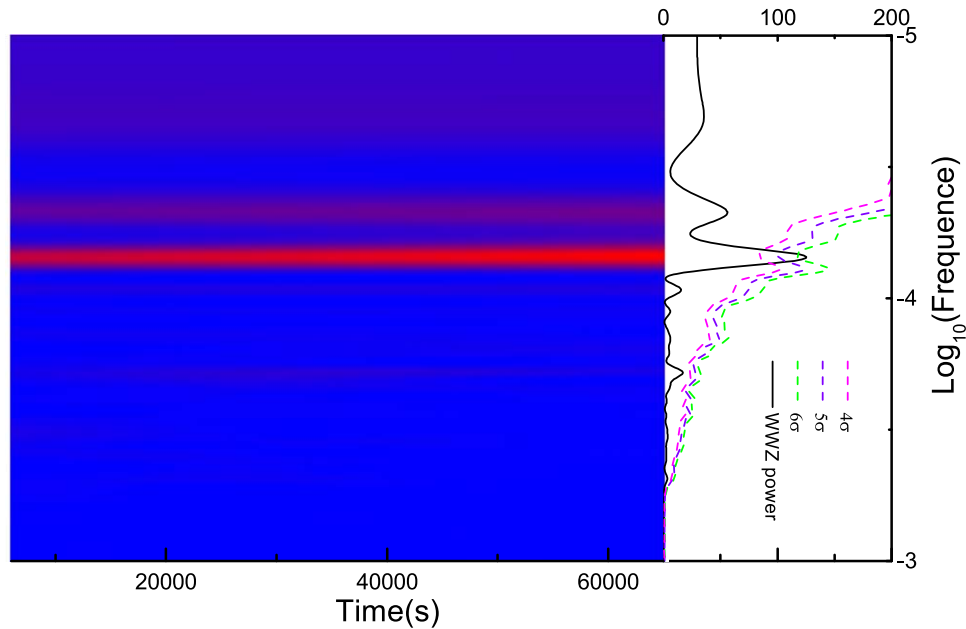


Figure 3. Left panel: 2D contour map of the WWZ power spectra of the total energy band of 0.3–10 keV light curve. Right panel: the average WWZ (black solid line) powers of the 0.3–10 keV band light curve. The pink dashed line, purple dashed line and green dashed line represent 4σ , 5σ and 6σ significance levels respectively.

time-averaged WWZ power spectrum and displays a higher significance level peak at the frequency $\sim 7.045 \times 10^{-5}$ Hz than 6σ . The REDFIT (Schulz & Mudelsee 2002) is also used to evaluate the significance of the PSD against the red-noise background. There is a $\sim 7.045 \times 10^{-5}$ Hz peak with a

confidence level of $>99\%$ (it is worth noting that the REDFIT code provides a maximum significance of 99%) and shown in Figure 4.

In order to analyze the origin of the QPO signal at 7.045×10^{-5} Hz deeply, we repeat these steps above to evaluate the

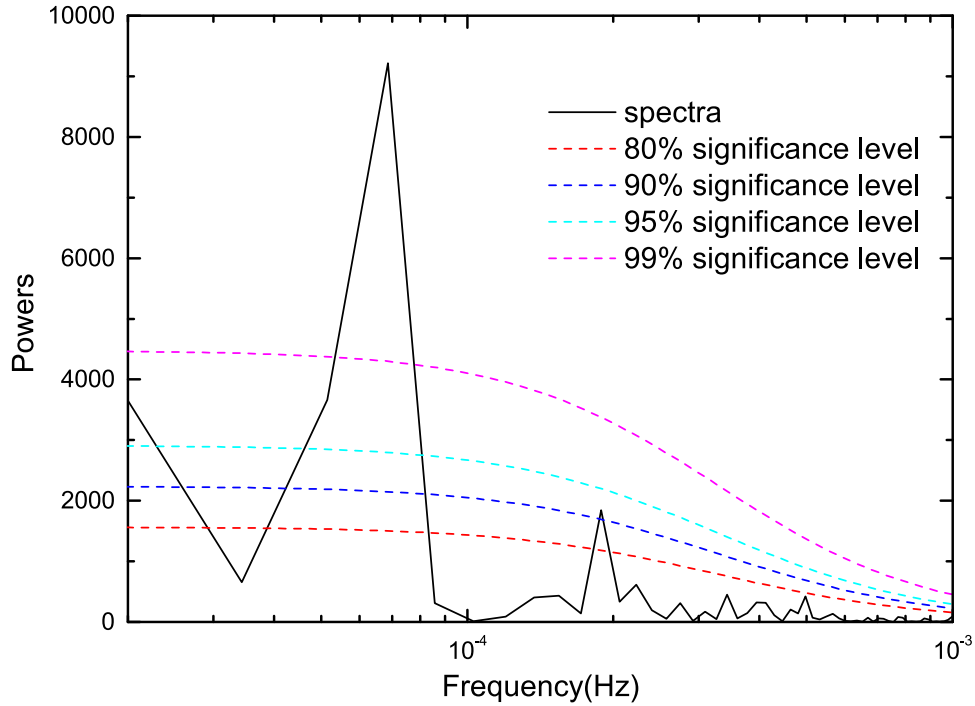


Figure 4. Result of the analysis by REDFIT for the 0.3–10 keV band light curve. The black solid line is bias-corrected power spectra. Dashed curves from bottom to top are the theoretical red-noise spectra, 80%, 90%, 95%, and 99% significance levels respectively.

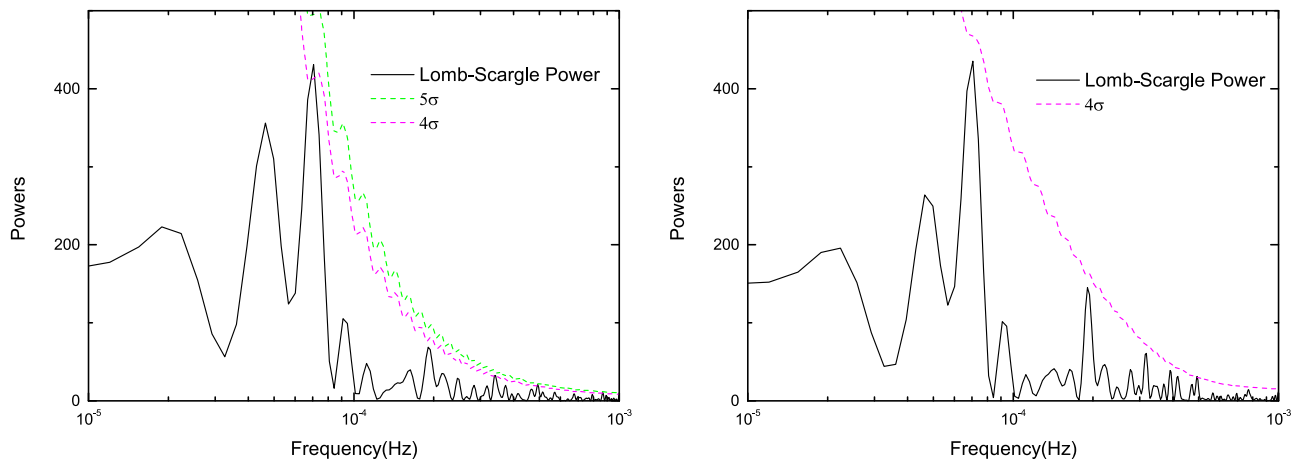


Figure 5. Left panel and Right panel are the LSP power spectra of 0.3–0.6 keV band and 0.6–1 keV band respectively and are shown in the black solid line. The 4σ (pink dashed line) and 5σ (green dashed line) significance level curves calculated based on the simulation of 10^5 light curves with the method of Emmanoulopoulos et al. (2013).

significance of QPOs at 0.3–0.6 keV, 0.6–1 keV, 1–3 keV and 3–10 keV and the results are shown as follows:

3.1. 0.3–0.6 keV

The left panel of Figure 5 shows that the confidence level of the QPO signal at 0.3–0.6 keV energy band is higher than 4σ by using the LSP method, but which is smaller than 5σ

obtained by the total energy band 0.3–10 keV. We still consider that the QPO signal should be existent larger than 4σ . Even more, the WWZ method gives a higher significance level of 6σ for the QPO signal of 0.3–0.6 keV shown by the left panel of Figure 7. The result of the analysis by REDFIT for the 0.3–0.6 keV (the left panel of Figure 9) shows an OPQ signal with a confidence of $>99\%$.

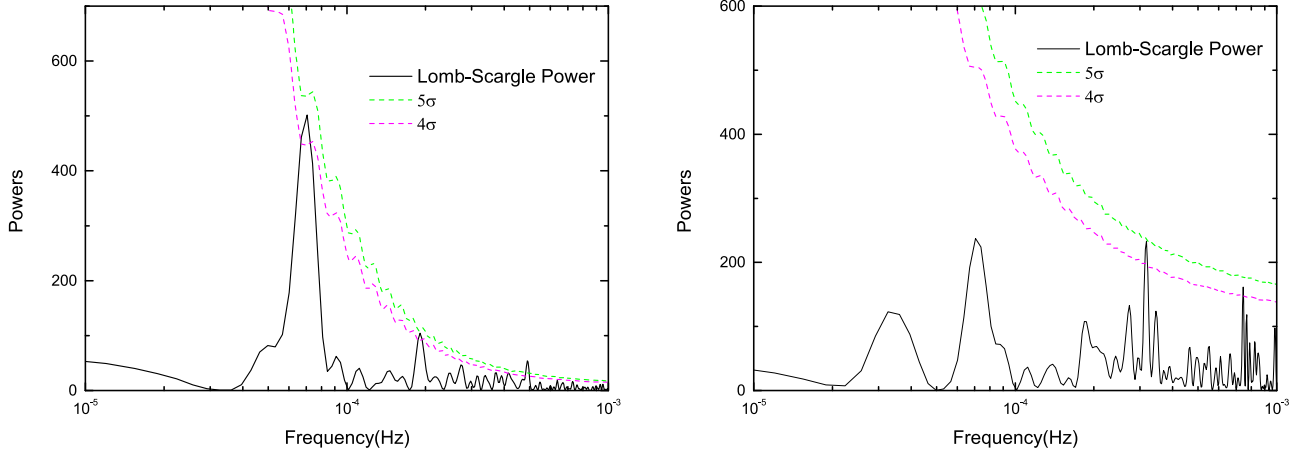


Figure 6. Left panel and Right panel are the LSP power spectra of 1–3 keV band and 3–10 keV band respectively and are shown in the black solid line. The 4σ (pink dashed line) and 5σ (green dashed line) significance level curves calculated based on the simulation of 10^5 light curves with the method of Emmanoulopoulos et al. (2013).

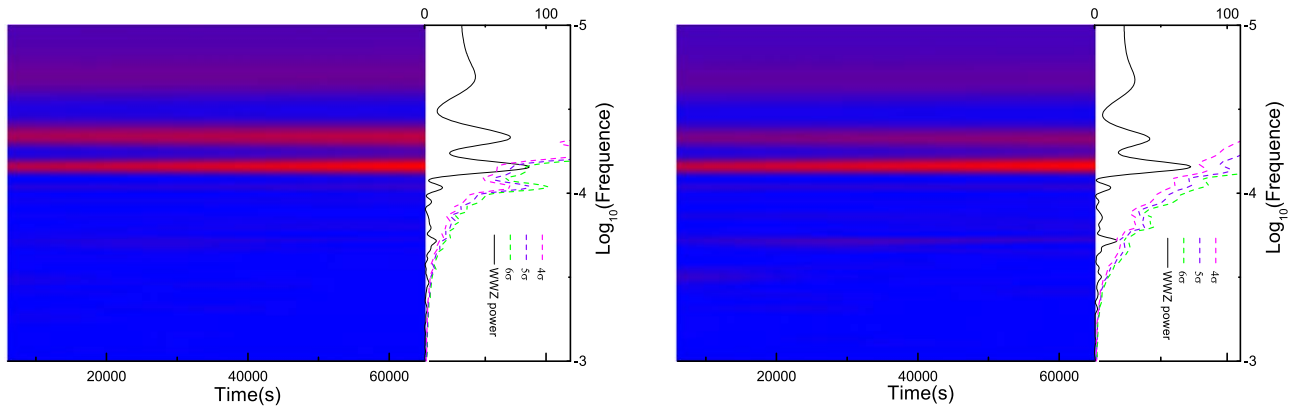


Figure 7. The power spectra of 0.3–0.6 keV and 0.6–1 keV band obtained by the WWZ method shown in the left panel and the right panel respectively. The pink dashed line, purple dashed line and green dashed line represent 4σ , 5σ and 6σ significance levels respectively.

3.2. 0.6–1 keV

The results of the analysis by LSP and WWZ methods show that there are nothing QPO signal at 0.6–1 keV energy band larger than the 4σ significance level shown in the right panel of Figures 5 and 7. The result by using the REDFIT method shows the significance level of the peak is larger than $>99\%$ (the right panel of Figure 9). However, the 99% significance level is less than 3σ , so we cannot determine the QPO signal by using the REDFIT method only.

3.3. 1–3 keV

The result of the analysis of the OPQ signal at the 1–3 keV energy band is similar with 0.3–0.6 energy band. The LSP method displays a QPO signal at 7.045×10^{-5} Hz larger than the 4σ significance level (seen in the left panel of Figure 6), and

the WWZ method gives a higher significance level of 6σ for the QPO signal (seen in the left panel of Figure 8). The result of the analysis by REDFIT for the 1–3 keV (seen in the left panel of Figure 10) shows a QPO signal at 7.045×10^{-5} Hz and a higher frequency about 1.88×10^{-4} Hz than a confidence of $>99\%$. However, the signal at $\sim 1.88 \times 10^{-4}$ Hz is not found by other methods such as LSP and WWZ methods, and the 99% significance level is less than 3σ , so we cannot determine the signal by using the REDFIT method as mentioned above.

3.4. 3–10 keV

The right panel Figure 6 does not show any signal at the 7.045×10^{-5} Hz less than the 4σ significance level. But, some peaks at the frequency higher than 7.045×10^{-5} Hz with more than the 4σ significance level. However, the WWZ method

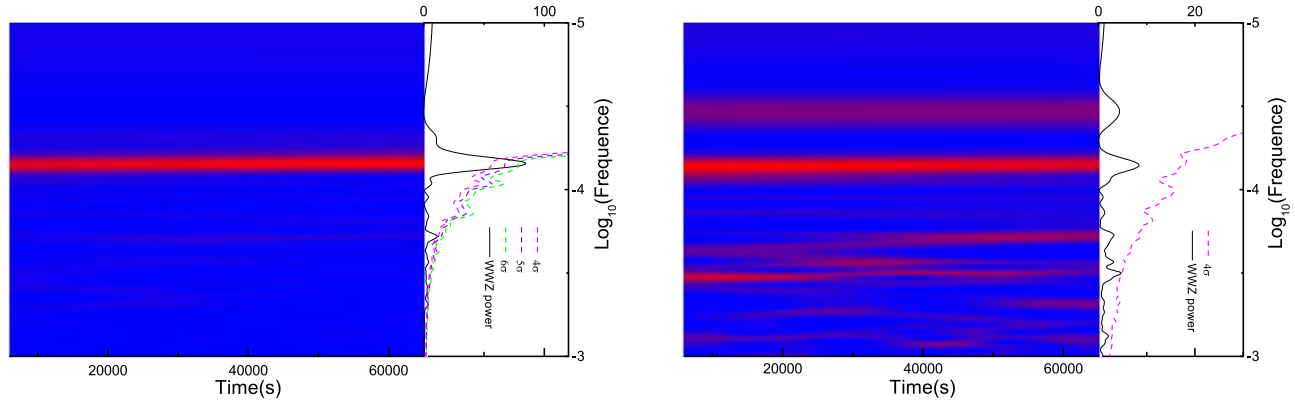


Figure 8. The power spectra of 0.3–0.6 keV and 0.6–1 keV band obtained by the WWZ method shown in the left panel and the right panel, respectively. The pink dashed line, purple dashed line and green dashed line represent 4σ , 5σ and 6σ significance level, respectively.

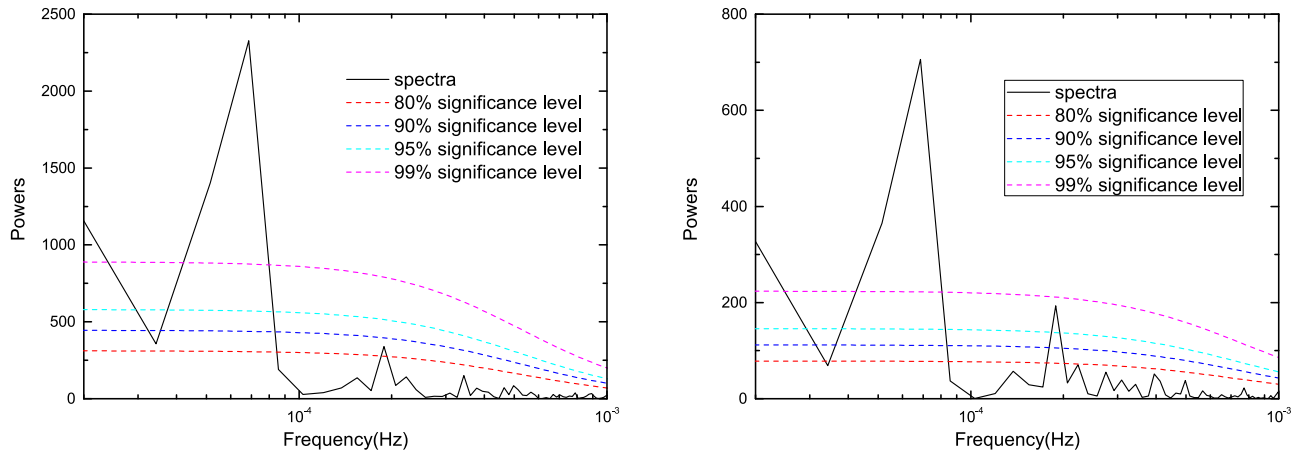


Figure 9. Result of the periodicity analysis by REDFIT for the 0.3–0.6 keV and 0.6–1 keV band light curve in the left panel and the right panel, respectively. The black solid line is bias-corrected power spectra. Dashed curves from bottom to top are the theoretical red-noise spectra, 80% 90%, 95% and 99% significance levels, respectively.

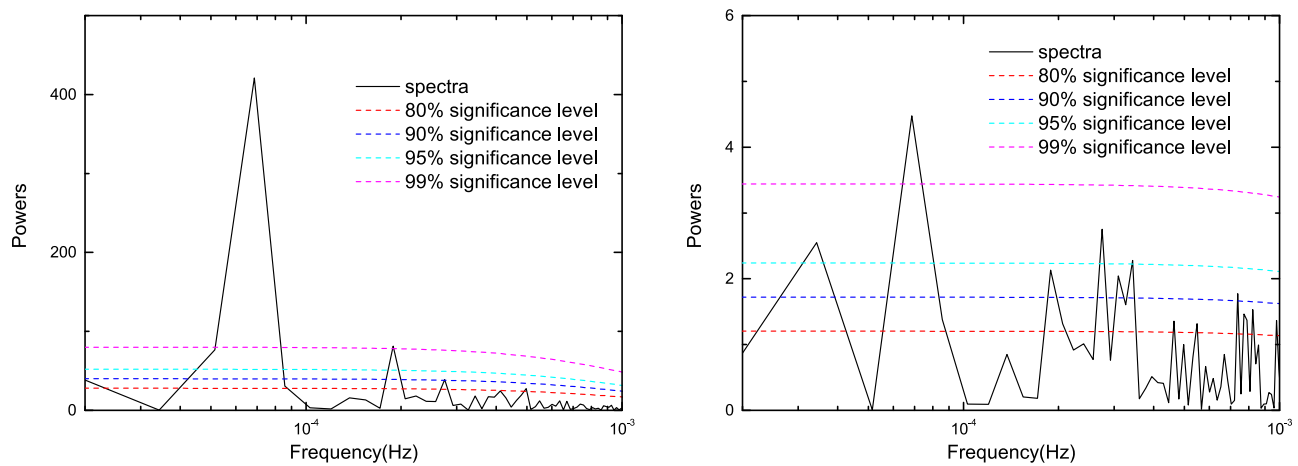


Figure 10. Result of the periodicity analysis by REDFIT for the 1–3 keV and 3–10 keV band light curve in the left panel and the right panel, respectively. The black solid line is bias-corrected power spectra. Dashed curves from bottom to top are the theoretical red-noise spectra, 80% 90%, 95%, and 99% significance levels, respectively.

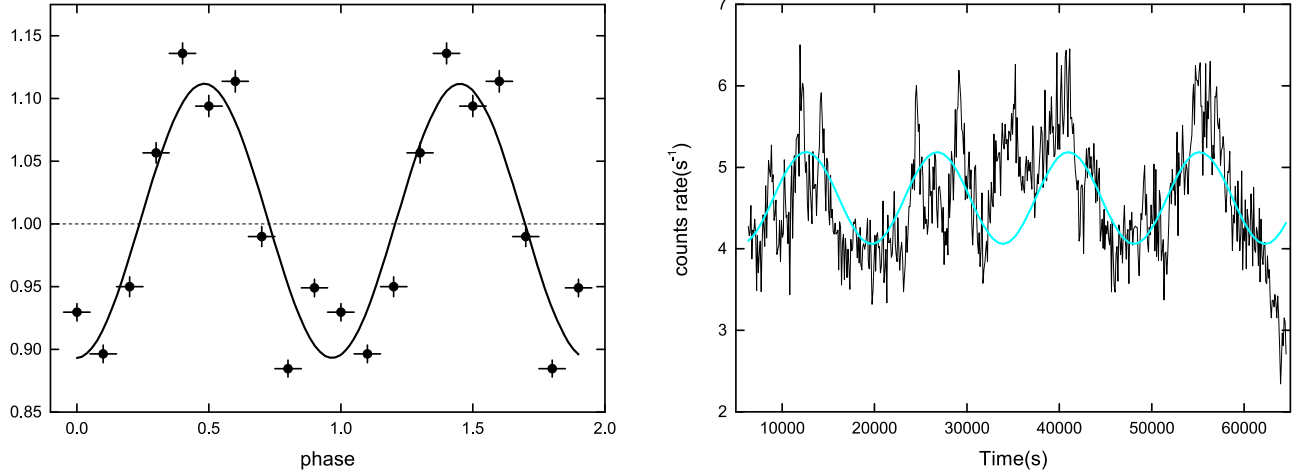


Figure 11. Left panel: the folded light curve of the total energy band 0.3–10 keV band with 7.045×10^{-5} Hz. Errors are propagated from the unfolded curve. The best-fit sinusoid is shown as the solid line and the mean count rate as the dashed line. Two cycles are plotted for clarity. Right panel: The best-fit sinusoid with the 0.3–10 keV light curve. The black line represents the light curve of 0.3–10 keV and the cyan line represents the best-fit sinusoid curve.

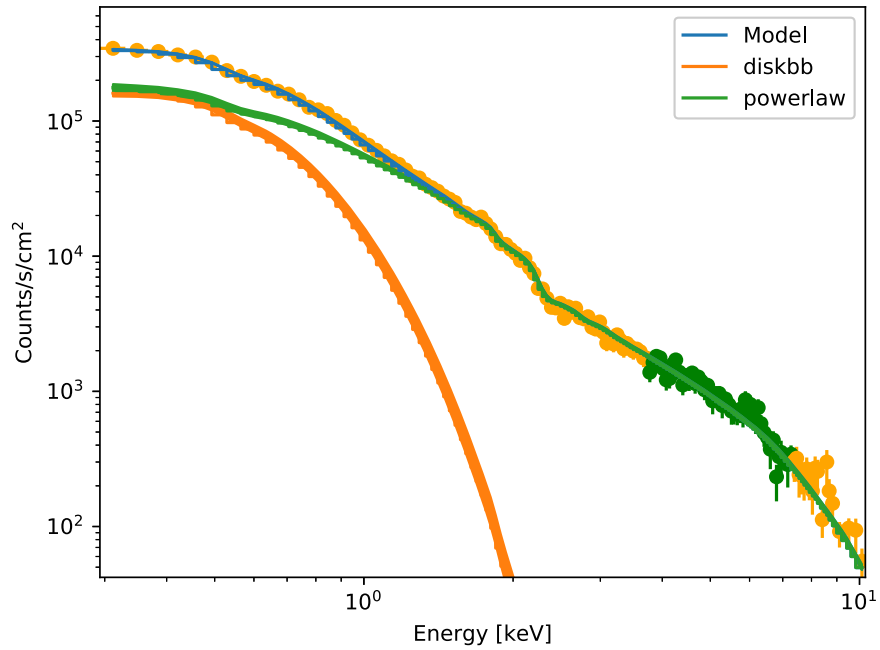


Figure 12. Fitting result obtained from BXA. The blue line means the best fitting result of the total model, the orange line means the diskbb component and the green line means the powerlaw component. The color of data point means the degree of the fitting, the fitting result of yellow data point is worse than the green data point.

does not only show nothing at those frequency (seen in the right panel Figure 8), but also at the 7.045×10^{-5} Hz with lower than the 4σ significance level. The REDFIT method still shows a QPO signal at 7.045×10^{-5} Hz with a confidence level of $>99\%$ (seen in the right of Figure 10), but the 99% significance level is less than 3σ , so we cannot determine the QPO signal by using the REDFIT method as mentioned above.

3.5. The Folded Light Curve Analysis for the Total Energy Band 0.3–10 keV

The folded light curve of 0.3–10 keV band with 7.045×10^{-5} Hz is shown in the left panel of Figure 11 with the best-fit sinusoid curve, which is also plotted with the light curve in the right panel of Figure 11. The periodic signal with

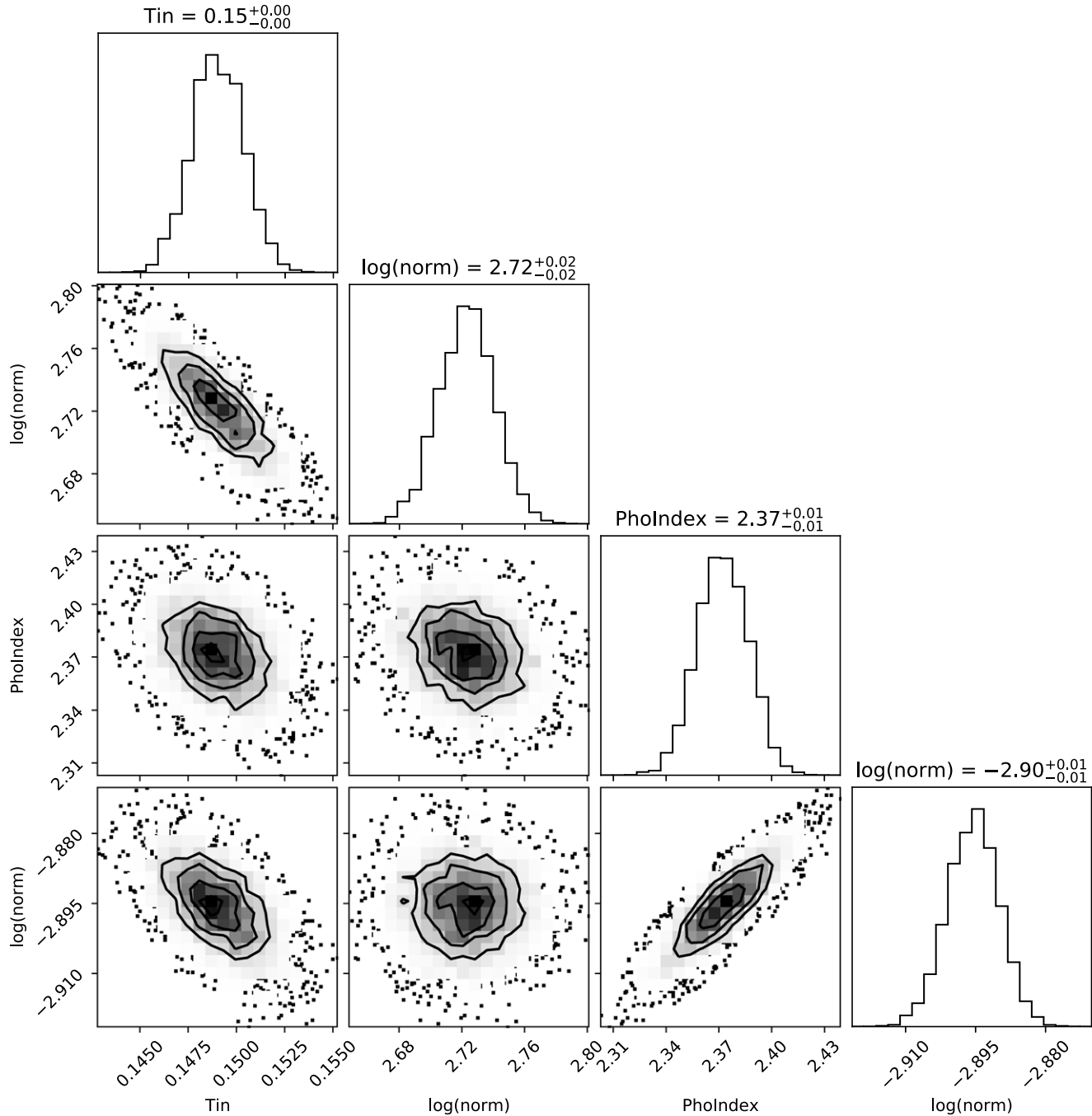


Figure 13. The corner plot of the model fitting obtained from BXA.

the frequency of 7.045×10^{-5} Hz is remarkable shown in Figure 11.

4. Spectral and Time Analysis

Through the above analysis, we find that a possible QPO signal at the 7.045×10^{-5} Hz in the total energy band

0.3–10 keV. From the deep analysis, the QPO signal could be generated in 0.3–0.6 and 1–3 keV energy bands. We first analyze the time-average spectra with XSPEC software (v12.11.1) (Arnaud 1996). In the soft X-ray band, the soft X-ray excess is the common component in many NSL1 galaxies, which maintain a stable temperature within a range of 0.1–0.2 keV for the blackbody spectrum of the accretion disk.

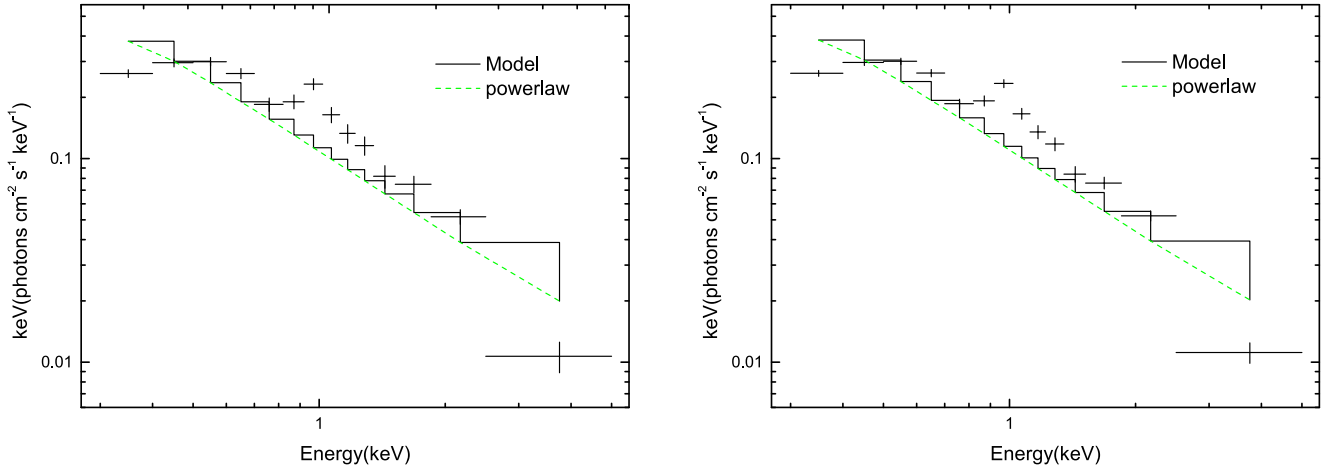


Figure 14. Fitting results of the absolute rms and covariance spectra in the left panel and the right panel respectively. The black line represents the fitting result and the green dashed line represents the powerlaw component. The diskbb component is too weak to display in these panels.

However, the origin of the soft X-ray excess in AGNs is as yet unknown. The hard X-ray has the power law spectrum and is generally considered to be from the inverse Compton scattering of the soft photons emitted from accretion disk in the hot corona. We use a phenomenological model to fit the spectrum as the following XSPEC form:

$$TBabs(diskbb + powerlaw)$$

where *TBabs* (Wilms et al. 2000) component is used to describe the Galactic absorption with setting the Galactic absorption hydrogen column density at $1.18 \times 10^{20} \text{ cm}^{-2}$ (Kalberla et al. 2005) during the spectral fitting with abundance set to *wilms* with *vern* cross-section by using *xset abund* and *xset xsect* command in XSPEC. *diskbb* component is used to describe the soft X-ray spectrum from an accretion disk consisting of multiple blackbody components. The *powerlaw* component is used to describe the spectrum of hard X-ray spectrum. In order to explore the best fit in the full range of parameter space of the model, the spectral fitting is performed using Bayesian X-ray analysis(BXA) (Buchner et al. 2014, 2019). BXA can use the fitting packages and models combined in XSPEC with UltraNest (Buchner 2021), a nested sampling algorithm. The priors could be the values to a reasonable parameter space, and posterior distributions can be examined after fitting to better understand the constraints that can be placed on parameters. The fitting result is shown in Figure 12 and the corner plot is shown in Figure 13 with the best fitting parameters obtained by the BXA analysis. The best fitting temperature of the soft X-ray excess has a typical value of 0.15 keV. However, the index ($\Gamma = 2.37_{-0.01}^{+0.01}$) of the powerlaw component is higher than the typical value about 1.8–2, which means the hot corona is weak. The different color data points in Figure 12 represent the degree of fitting in which the green data points is fitted better than the yellow ones. The different color data points in the hard X-ray energy band means

that the hot corona has complex structure in which some part of hot corona may generate the QPO signal at 1–3 keV, and the other part has non-signal at 3–10 keV.

We then use the model to fit the absolute rms and covariance spectra of the QPO signal at $7.045 \times 10^{-5} \text{ Hz}$ with the best fitting parameters obtained by BXA. We fix all model parameters except the normalization of each model component, in which we assume each model component to have same variability, so we can only change the normalization to fit the absolute rms and covariance spectra shown in Figure 14.

The rms and covariance spectra have the same spectral shape except different errors merely. The result of fitting the absolute rms and covariance spectra show the main component of the variability spectrum is the *powerlaw* spectra and soft X-ray excess does not contribute to the rms and covariance spectra because the *diskbb* is ignored, which means the QPO mainly comes from the hard X-ray hot corona even though in the soft X-ray energy band at 0.3–0.6 keV.

5. Discussion and Conclusions

The QPO is a very interesting phenomenon which contains some unknown physical mechanism. Generally, it is widely observed in BHXBs at both low frequency ($\sim 0.1\text{--}30 \text{ Hz}$) and high frequency ($\sim 40\text{--}450 \text{ Hz}$), where the low-frequency QPO could be generated by the Lense–Thirring precession and the high-frequency QPO could be related to the Keplerian period of the innermost disk. However, the QPOs are rarely detected in AGNs because their timescales are much longer than those of BHXBs. For many typical AGNs with BH masses of $10^{7-8} M_{\odot}$, their QPO signals are not easily observed, but the NLS1 with lower masses and high accretion rate could have the detected QPOs. Based on the methods of LSP, WWZ and REDFIT, we find a possible QPO signal at $\sim 7.045 \times 10^{-5} \text{ Hz}$ with 5σ , 6σ

and $>99\%$ confidence levels respectively in the total energy band 0.3–10 keV. In order to analyze the QPO signal deeply, we calculate the significance level of the QPO signal in 0.3–0.6 keV, 0.6–1 keV, 1–3 keV and 3–10 keV respectively by using the same method mentioned above. The QPO signal in 0.3–0.6 keV and 1–3 keV is obtained the significance level of 4σ by the LSP method and obtained by the WWZ method with 6σ . The REDFIT method shows a significant QPO signal in all energy band with the confidence level of $>99\%$, but the 99% confidence level is less than 3σ , so we cannot determine the QPO signal by using the REDFIT method. Therefore, we consider the QPO signal of the total energy band of 0.3–10 keV could be mainly contributed from 0.3–0.6 keV to 1–3 keV. Some peaks at the frequency above 7.045×10^{-5} Hz are shown in Figures 5 and 6, and the significance level is larger than 4σ , even higher than 5σ in the left panel of Figure 6, which display the LSP power spectra of 1–3 keV. But, these peaks vanish by using the WWZ and REDFIT methods with the significance level less than 4σ and $<99\%$ respectively. So, we consider these peaks at the higher frequency than 7.045×10^{-5} Hz are the false signal. Then, we use a phenomenological model to fit the spectrum for 0.3–10 keV by analyzed with BXA. The fitting result shows that the model could reproduce the total spectrum well and the fitting of the hard X-ray in about 4–7 keV is better, which may reveal the hard X-ray has a complex component. So we consider the QPO signal comes from a certain part of the hot corona which dominates the radiation in the 1–3 keV energy band. The *diskbb* indicates Mrk142 has a typical soft X-ray excess component with the temperature of 0.15 keV. However, the index of powerlaw is rather larger than a typical value about ~ 1.8 . It may display the corona of Mrk142 is weak and reveal that the special form of the hot corona may generate the QPO signal. We will study this characteristic in the future by using the NuSTAR data. The analysis of the absolute rms and covariance spectra fitting show that the QPO signal could come from the hot corona rather than the soft X-ray excess. Therefore, the QPO signal in 0.3–0.6 keV energy band is also generated from the hot corona. The high significant QPO of RE J1034+396 at 2.7×10^{-4} Hz is widely accepted so far. Interestingly, the property of the QPO found in Mrk 142 is different from that in RE J1034+396 although both AGNs have similar black hole masses, and the QPO frequency of Mrk142 is smaller an order of magnitude than RE J1034+396. It implies that two AGNs have different origins of the QPOs.

Acknowledgments

We thank the anonymous referee for helpful suggestions and comments. We appreciate Dr. Dahai Yan and Dr. Pengfei Zhang for their useful suggestions. We acknowledge the financial supports from the Science Foundation of Department of Education of Yunnan Province (2024J0935). Y.C. is grateful for funding for the training Program for talents in Xingdian, Yunnan Province.

References

- Alston, W. N., Parker, M. L., Markevičiūtė, J., et al. 2015, *MNRAS*, 449, 467
 Alston, W. N., Markevičiūtė, J., Kara, E., et al. 2014, *MNRAS*, 445, L16
 Ackermann, M., Ajello, M., Albert, A., et al. 2015, *ApJL*, 813, L41
 Arnaud, K. A. 1996, *ASPC*, 101, 17
 Bhatta, G. 2017, *ApJ*, 847, 7
 Bhatta, G., Zola, S., Stawarz, L., et al. 2016, *ApJ*, 832, 47
 Buchner, J. 2021, *JOSS*, 6, 3001
 Buchner, J., Brightman, M., Nandra, K., et al. 2019, *A&A*, 629, A16
 Buchner, J., Georgakakis, A., Nandra, K., et al. 2014, *A&A*, 564, A125
 Carpano, S., & Jin, C. 2018, *MNRAS*, 477, 3178
 Emmanoulopoulos, D., McHardy, I. M., & Papadakis, I. E. 2013, *MNRAS*, 433, 907
 Espaillat, C., Bregman, J., Hughes, P., et al. 2008, *ApJ*, 679, 182
 Fan, J. H., Kurtanidze, O., Liu, Y., et al. 2014, *ApJS*, 213, 26
 Foster, G. 1996, *AJ*, 112, 1709
 Gierliński, M., Middleton, M., Ward, M., et al. 2008, *Natur*, 455, 369
 González-Martín, O., & Vaughan, S. 2012, *A&A*, 544, A80
 Graham, M. J., Djorgovski, S. G., Stern, D., et al. 2015, *Natur*, 518, 74
 Gupta, A. C., Srivastava, A. K., & Wiita, P. J. 2009, *ApJ*, 690, 216
 Gupta, A. C., Tripathi, A., Wiita, P. J., et al. 2018, *A&A*, 616, L6
 Hong, S., Xiong, D., & Bai, J. 2018, *AJ*, 155, 31
 Hu, C.-P., Chou, Y., Yang, T.-C., et al. 2014, *ApJ*, 788, 31
 Jansen, F., Lumb, D., Altieri, B., et al. 2001, *A&A*, 365, L1
 Jin, C., Done, C., & Ward, M. 2020, *MNRAS*, 495, 3538
 Kalberla, P. M. W., Burton, W. B., Hartmann, D., et al. 2005, *A&A*, 440, 775
 King, O. G., Hovatta, T., Max-Moerbeck, W., et al. 2013, *MNRAS*, 436, L114
 Kushwaha, P., Sarkar, A., Gupta, A. C., et al. 2020, *MNRAS*, 499, 653
 Lachowicz, P., Gupta, A. C., Gaur, H., et al. 2009, *A&A*, 506, L17
 Li, X.-P., Cai, Y., Yang, H.-T., et al. 2021, *MNRAS*, 506, 1540
 Li, X.-P., Luo, Y.-H., Yang, H.-Y., et al. 2017, *ApJ*, 847, 8
 Li, Y.-R., Songsheng, Y.-Y., Qiu, J., et al. 2018, *ApJ*, 869, 137
 Lin, D., Irwin, J. A., Godet, O., et al. 2013, *ApJL*, 776, L10
 Lomb, N. R. 1976, *Ap&SS*, 39, 447
 Mancuso, G. C., Altamirano, D., García, F., et al. 2019, *MNRAS*, 486, L74
 Pan, H.-W., Yuan, W., Yao, S., et al. 2016, *ApJL*, 819, L19
 Porquet, D., Reeves, J. N., O'Brien, P., & Brinkmann, W. 2004, *A&A*, 422, 85
 Sandrinelli, A., Covino, S., Dotti, M., et al. 2016, *AJ*, 151, 54
 Sandrinelli, A., Covino, S., & Treves, A. 2014, *ApJL*, 793, L1
 Scargle, J. D. 1982, *ApJ*, 263, 835
 Schulz, M., & Mudelsee, M. 2002, *CG*, 28, 421
 Wilms, J., Allen, A., & McCray, R. 2000, *ApJ*, 542, 914
 Xiong, D., Bai, J., Zhang, H., et al. 2017, *ApJS*, 229, 21
 Yang, S., Yan, D., Zhang, P., et al. 2021, *ApJ*, 907, 105
 Zhang, H., Yan, D., Zhang, P., et al. 2021, *ApJ*, 919, 58
 Zhang, J., Zhang, H.-M., Zhu, Y.-K., et al. 2017, *ApJ*, 849, 42
 Zhang, P., & Wang, Z. 2021, *ApJ*, 914, 1
 Zhang, P., Zhang, P. F., Yan, J. Z., et al. 2017, *ApJ*, 849, 9
 Zhang, P. F., Zhang, P., Liao, N. H., et al. 2018, *ApJ*, 853, 193